Catalysis Today 138 (2008) 124–129

Contents lists available at ScienceDirect

Catalysis Today

journal homepage: www.elsevier.com/locate/cattod

Low temperature hydrogen production from methane on cerium nickel- and zirconium-based oxyhydrides

L. Jalowiecki-Duhamel *, H. Zarrou, A. D'Huysser

UCCS Unité de Catalyse et de Chimie du Solide, UMR CNRS 8181, Bât. C3, Université des Sciences et Technologies de Lille, 59655 Villeneuve d'Ascq Cedex, France

ARTICLE INFO

Article history:
Available online 23 July 2008

Keywords:
Anionic vacancy Ceria
Hydrogen production
Methane partial oxidation
Oxyhydride
Nickel oxide

ABSTRACT

Hydrogen production from methane has been obtained at low temperature, in presence of O_2, over cerium nickel and zirconium $CeZr_zNi_xO_y$ ($z = 0$ or 0.5 and $0 < x \leq 3$) oxyhydrides. A H_2 yield of 100% is obtained at high temperature (650 °C), at 200 °C a yield of 34% is reached with a stable methane conversion at 53% and selectivity in H_2 at 64% when the solid is previously in situ treated in H_2 at 200 °C. Different physicochemical techniques have been used to characterize the catalysts. Depending on the composition and metal loading, a solid solution and/or a highly dispersed nickel oxide in ceria (or ceria–zirconia) can be obtained. Ion sputtering followed by XPS analysis has been very useful for estimating the size of small NiO clusters (10–15 Å) present in the compounds. Correlations among the species present in the solid, and the catalytic performances are discussed, an active site based on the formation of anionic vacancies and a mechanism involving a heterolytic abstraction of a hydride species from methane are proposed.

1. Introduction

Synthesis gas ($H_2 + CO$) is industrially produced through the steam reforming of methane (endothermic reaction) at high temperature. However, catalytic partial oxidation of methane (POM) offers the greatest potential to hydrogen or synthesis gas because adoption of POM would result in energy savings, due to mild exothermicity. Moreover, the hydrogen purified after a CO clean-up process can be used for ammonia synthesis, hydrotreating processes and reduction operations in metallurgical industry. Another very interesting use of hydrogen is based on its conversion into power in fuel cell systems. Recently, there has arisen a strong interest in using H_2-based fuel cells as future energy carrier due to the high conversion efficiency of hydrogen energy to electricity as well as no emissions of pollutant gases.

Ni metal or noble metals, are often used as catalytically active components for POM. Many research groups have developed various Ni catalysts effective for the reaction because of a high cost of noble metals. CeO_2–NiO catalysts have been studied in many oxidation reactions by taking advantage of ceria redox properties that can be enhanced by adding Zr and forming solid solutions (CeO_2–ZrO_2). It has also been reported that a good coking resistance depends on a high dispersion of Ni [1,2]. Therefore, among the important parameters pointed out, the catalysts dispersion and reducibility are often taken into consideration [1–4]. Besides, the catalysts are required to work under various conditions, and improvement in the stability of the catalysts is desired, in particular, in strong reducing conditions. In some cases the results have been ameliorated with a CH_4/O_2 ratio higher than 2 [5]. Moreover, the effect of an activation step has also been noted, Choudhary et al. found that after catalytic reaction at high temperature, NiO–Yb_2O_3 allowed to obtain at 298 °C a methane conversion of 71% with a CO and H_2 selectivity, respectively, of 84 and 88% [6].

In this paper, we investigate the partial oxidation of CH_4 to H_2 and CO in strong reducing conditions ($CH_4/O_2 = 3$) over cerium nickel and zirconium $CeZr_{0.5}Ni_xO_y$ mixed oxides in situ activated in H_2 (oxyhydrides). We report studies of their structural, dispersion and reduction properties in order to find a relationship with catalytic reaction and propose an active site.

2. Experimental methods

The mixed oxides denoted $CeZr_zNi_xO_y$ ($z = 0$ or 0.5 and $0 < x \leq 3$) where x and z are the Ni/Ce and Zr/Ce atomic ratios, respectively, were prepared by coprecipitation of the corresponding hydroxides from mixtures of cerium zirconium and nickel nitrates (0.5 M) using triethylamine (TEA) as a precipitating agent.

* Corresponding author. Tel.: +33 3 20 33 77 35; fax: +33 3 20 33 65 61.
E-mail address: louise.duhamel@univ-lille1.fr (L. Jalowiecki-Duhamel).

0920-5861/$ – see front matter © 2008 Elsevier B.V. All rights reserved.
doi:10.1016/j.cattod.2008.06.011

After filtration, the solids are dried at 100 °C and calcined in air at 500 °C for 4 h [7]. The loading has been measured by microanalysis.

The catalytic partial oxidation of CH_4 was performed with 0.2 g of catalyst under atmospheric pressure in a fixed-bed stainless-steel tubular reactor by cofeeding the nitrogen-diluted reaction gases ($CH_4/O_2/N_2$ = 3/1/3). Each catalyst was diluted with SiC (1:1). The total flow rate was 3 L h^{-1} (down flow) and the reaction temperature, measured in the catalytic bed with a thermocouple, was in the range of 50–700 °C. The experimental details have been published previously [8]. The gases at the outlet of the reactor were analyzed by FID and TCD gas chromatography. Conversion (CH_4, O_2) and selectivity (H_2, CO, CO_2) were collected after about 5 h of reaction when the steady state conversion and selectivity were obtained for each temperature. Carbon and H_2O are also formed but the quantity has not been analyzed. Conversion (X), selectivity (S) and yield (Y) were calculated as follows:

$$X_{CH_4} = \frac{CH_4^{in} - CH_4^{out}}{CH_4^{in}}, \qquad X_{O_2} = \frac{O_2^{in} - O_2^{out}}{O_2^{in}},$$

$$Y_{H_2} = \frac{H_2^{out}}{2CH_4^{in}}, \qquad S_{H_2} = \frac{Y_{H_2}}{X_{CH_4}}, \qquad S_{CO} = \frac{Y_{CO}}{X_{CH_4}}, \qquad S_{CO_2} = \frac{Y_{CO_2}}{X_{CH_4}}$$

X-ray powder diffraction (XRD) analysis was carried out with a D 5000 Siemens diffractometer using a copper target and a secondary beam monochromator. The XRD patterns were registered in the 2θ domain (15–80°) with a measured step of 0.02°. The Kα_2 contribution was eliminated from the diffraction by computer post-processing; the patterns obtained were not subjected to other treatments. The crystallites size was calculated using the Scherrer equation, from the most intense reflections observed for the NiO and CeO_2 crystallographic structures: (1 1 1), (2 0 0), and (2 2 0).

Temperature-programmed reduction (TPR) was performed on a Micrometrics Autochem 2920 analyser, and hydrogen consumption was measured by a TCD detector: 25 mg of the sample was treated in the 5% H_2–95% Ar gas mixture (2 L/h). The temperature was increased to 800 °C at a heating rate of 10 °C/min. To calibrate the amount of H_2 consumption, the AgO powder was used.

The X-ray photoelectron spectroscopy (XPS) spectra of the samples were obtained on a VG Escalab 220 XL instrument using Al Kα radiation ($h\nu$ = 1486.6 eV). The anode was operated at a power of 300 W and the fixed retardation ratio (FRR) was applied. The base pressure attained during the analysis was 1.33×10^{-6} Pa. The calcined samples, lightly pressed on an Au-holder, were applied to a sample rod. For calibration of the binding energy (E_B) scale of photoemission features, the Ce 3d u‴ peak at 916.7 eV was taken as an internal reference. In our experimental conditions, the reproducibility of E_B was estimated at ±0.2 eV. As for atomic ratios, they were calculated by assuming a homogeneous distribution of the catalyst components. The details of the spectrometer and the experimental procedure are given in Ref. [9].

The spectrometer allows ions to be bombarded directly onto the surface of compounds. For this, the solids were thinly pressed on an indium-holder and measurements were performed with the same analysis conditions as those previously described. Ions sputtering conditions were carried out with an ionic energy of 2000 eV and an applied tension of 580 V. The cumulated time of sputtering treatment under argon ions was varied from 1 to about 5000 s.

3. Results and discussion

3.1. XRD

Fig. 1 reports the diffraction patterns obtained with different $CeZr_{0.5}Ni_xO_y$ solids. Only a ceria like phase is apparent in every solid analyzed (34-0394 JCPDS file) while crystallized NiO (4-0835 JCPDS file) appears when $x \geq 0.5$. No phase related to the presence of Zr has been observed. The $CeNi_xO_y$ mixed oxides were classified in two families, depending on the nickel content: the first family with $x \leq 0.5$ corresponds to a solid solution with the substitution of Ni^{2+} ions in the CeO_2 lattice and the second family with $x > 0.5$ concerns compounds in which crystallized NiO and solid solution coexist [10–12]. The size of the nickel oxide varies considerably from clusters to a crystallized material depending on the x-value and the experimental conditions (preparation conditions, calcination temperature, etc.). As already reported in previous studies for $CeNi_xO_y$ compounds, a careful examination of the patterns shows that the addition of nickel affects not only the broadness of the ceria peaks, but also their position (Fig. 2), attributed to the substitution of Ce^{4+} cations by Ni^{2+} cations inside the CeO_2 lattice and interpreted by the formation of a cerium–nickel solid solution [12]. As a matter of fact, the nickel ionic radius (Ni^{2+}: 0.7 Å), is smaller than the cerium ionic radius (Ce^{4+}: 0.9 Å). It has been reported on binary mixed oxides, that the highest proportion of solid solution has been obtained for the $CeNi_{0.5}O_y$ compound, as also observed here when the molar ratio $Ni/M_T = 0.3$ (M_T = Ni + Ce + Zr, $Ni/M_T = x/(1 + z + x)$ with z = 0 or 0.5). The results obtained on $CeZr_{0.5}Ni_xO_y$ compounds reported in Fig. 2 show clearly that the presence of Zr affects even more drastically the ceria phase forming a well-known solid solution allowed by the size of Zr^{4+} cations (0.84 Å).

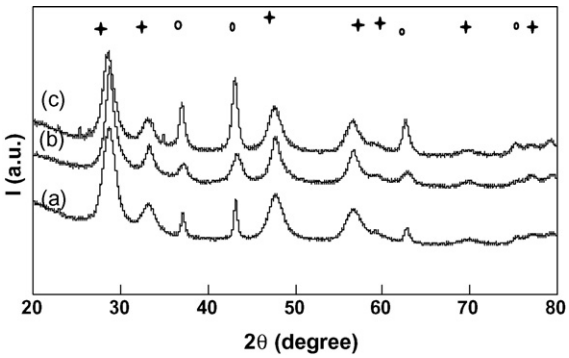

Fig. 1. XRD patterns of (a) $CeZr_{0.5}Ni_1O_y$ (b) $CeZr_{0.5}Ni_2O_y$ and (c) $CeZr_{0.5}Ni_3O_y$ compounds: CeO_2 (✦) and NiO (○).

The grain size (d) has been estimated from the XRD line widths taking into account the (1 1 1), (2 0 0) and (2 2 0) peaks, for both NiO and CeO_2. The average dimensions obtained for $CeZr_{0.5}Ni_1O_y$ and $CeNi_1O_y$ oxides are summarized in Table 1. The size of the crystallites of the mixed oxides is found smaller than the size measured for the pure oxides [12]. This phenomenon has been

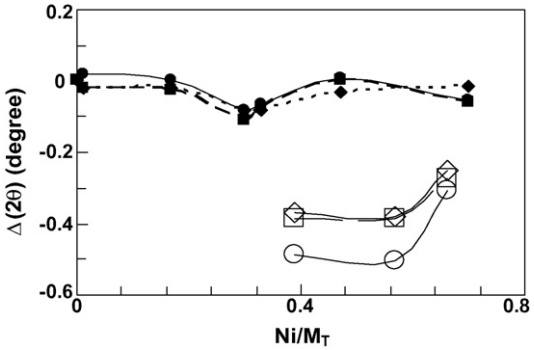

Fig. 2. Shift of the CeO_2 diffraction peaks in $CeZr_{0.5}Ni_xO_y$: (○) (1 1 1), (□) (2 0 0), (△) (2 2 0) and $CeNi_xO_y$: (●) (1 1 1), (■) (2 0 0), (▲) (2 2 0). $\Delta(2\theta)$ = (peak position of the reference oxide CeO_2) − (peak position of the CeO_2-like phase in the mixed oxide). ($Ni/M_T = x/(1 + z + x$; z = 0 or 0.5).

Table 1
Surface area (BET) and crystallite size (calculated from the Scherrer equation)

Catalyst	Ni (wt.%)	Ni/M_T	S.A. ($m^2\ g^{-1}$)	d CeO_2 (Å)	d NiO (Å)
NiO	78.6	1	25	–	>200
CeO_2	0	0	89	97	–
$CeNi_1O_y$	22.1	0.47	105	46	96
$CeZr_{0.5}Ni_1O_y$	19.3	0.39	113	46	118

explained by an increase of the crystallographic disorder in the mixed oxides. This technique allows an estimation of the crystallites size at about 50 Å for CeO_2-like species and at about 100 Å for NiO species. However, it is important to recall that crystallites with a size smaller than 20 Å cannot be detected by XRD (because of the limits of detection).

3.2. XPS

Cerium compounds have XPS spectra with rather complex features due to numerous initial and final 4f electronic configurations. According to Barr [13], the 3d spectrum, registered on pure ceria, can be resolved into three spin–orbits doublets $3d_{3/2}$–$3d_{5/2}$, respectively, denoted (u, v), (u″, v″) and (u‴, v‴). As for the $CeNi_xO_y$ solids already studied by this technique in the laboratory [9], these characteristics are well visualized on the Ce 3d spectra, presented in Fig. 3 on $CeNi_1O_y$ and $CeZr_{0.5}Ni_1O_y$ compounds, and one can unambiguously ascribe the 3d envelope to Ce^{4+} cations in CeO_2-like species. O1s lines of the compounds have all binding energies of 529.1 ± 0.1 eV, showing without doubt that the oxygen element is characteristic of some typical O^{2-} lattice oxygen species. Moreover, Fig. 3 shows the Ni $2p_{3/2}$ band shapes of the mixed oxides which have been analyzed in a similar manner as reported previously [9]. A careful examination of these band shapes has been performed and a line broadening effect is observed when the nickel content increases. As already published in previous works on cerium-based compounds, it can be admitted that Ni^{2+} species mainly form a solid solution with ceria and with ceria–zirconia. For higher Ni/Ce ratios several types of surface nickel seem to coexist, in agreement with XRD [9,12]. Therefore, the system can be described as a solid solution of nickel in ceria or in ceria–zirconia in close contact with nickel oxide. However, some quantitative XPS features provide additional information. Superficial nickel compositions of the mixed oxides determined from XPS atomic ratios, are compared to bulk nickel content (elemental analysis) in Fig. 4. The 45° diagonal line corresponds to the case of a homogeneous distribution of nickel inside the solid, and rather good results are obtained on the ternary compounds. By comparison, a $CeNi_{0.5}O_y$ sample prepared by coprecipitation in KOH, calcined at 300 °C, has already been reported

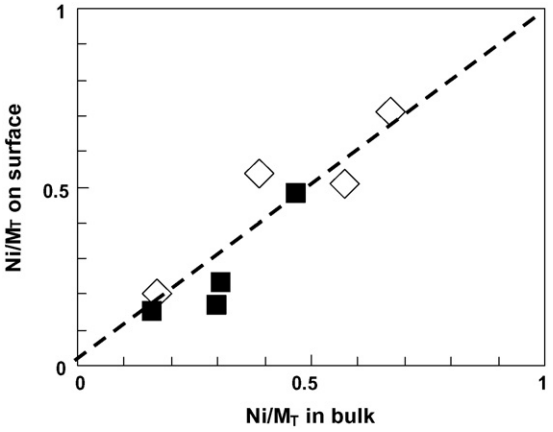

Fig. 4. Variation of Ni/M_T surface ratio as a function of Ni/M_T bulk ratio in the $CeNi_xO_y$ (■) and $CeZr_{0.5}Ni_xO_y$ (◇) series.

to give the best homogeneous distribution of nickel, in agreement with a maximal incorporation of Ni^{2+} cations inside the ceria lattice [12].

Ions sputtering in combination with surface analysis techniques such as XPS provide information on the in-depth distribution of elements inside the solid. This technique has found many applications in materials that show some composition inhomogeneity in their topmost layers and has been previously detailed and applied in our laboratory to characterize the $CeNi_xO_y$ compounds [9]. The decrease of the superficial Ni/Ce intensities ratio versus the sputtering cumulated time is presented in Fig. 5 for $CeNi_1O_y$ and $CeZr_{0.5}Ni_1O_y$ catalysts. During the first minute of sputtering there is a decrease of the Ni/Ce ratio, confirming that the structure does not correspond to a homogeneous solid solution, and in agreement with the presence of small crystallites in strong interaction with some bigger aggregates. In order to estimate the size of the NiO crystallites on the support, two models have been suggested, allowing simplifying the problem in two extreme cases, taking into account or not the presence of a solid solution of nickel in ceria. Despite the fact that these two cases describe a very simple structure of the catalysts, they allow the calculation of the particles size by default and by excess. The results obtained using these models are summarized in Table 2, showing an increase of the NiO crystallite size when the solid solution is taken into account. In this case, the size of the NiO crystallites is estimated to be between 5 and 15 Å for the studied compounds. The presence of small NiO clusters is also found with a low Ni content in $CeZr_{0.5}Ni_{0.3}O_y$. Clearly some small NiO clusters are always present, they are smaller than the ceria grains size and coexist with the solid

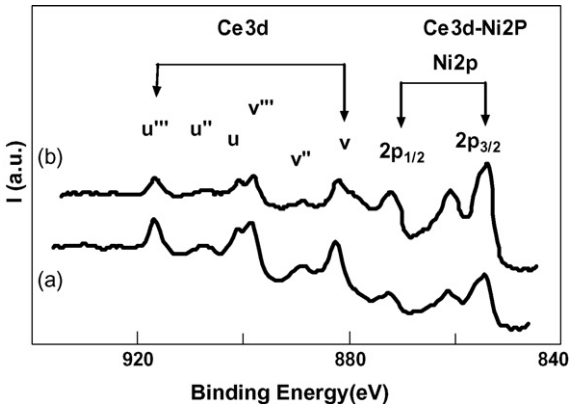

Fig. 3. Ce 3d and Ni $2p_{3/2}$ XPS spectra of (a) $CeNi_1O_y$ and (b) $CeZr_{0.5}Ni_1O_y$.

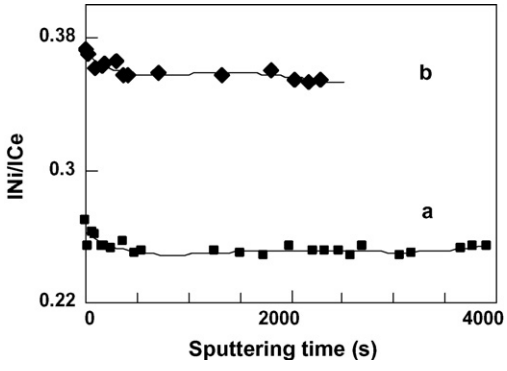

Fig. 5. Ni/Ce surface intensities ratio as a function of the bombardment time under argon ions on (a) $CeNi_1O_y$ and (b) $CeZr_{0.5}Ni_1O_y$.

Table 2
Estimation of NiO crystallites size by depth sputtering followed by XPS[a]

Solid solution	Particle size (Å)[a]		
	$CeZr_{0.5}Ni_{0.3}O_y$	$CeZr_{0.5}Ni_1O_y$	$CeNi_1O_y$
Without	4	5	12
With	12	8	15

[a] Detailed and applied on similar compounds in Ref. [9].

solution for low Ni contents, and with larger NiO crystallites, observed by XRD, for higher Ni contents.

Strong interactions between cerium zirconium and nickel are apparent in the compounds. These interactions are located either inside the fluorite lattice (ceria or ceria–zirconia) or at the interface between NiO crystallites and these ceria and/or ceria–zirconia grains.

3.3. TPR in H_2

The TPR profiles in H_2 of the $CeZr_{0.5}Ni_1O_y$ solids are shown in Fig. 6. At about 275 °C, a first maximum temperature reduction peak is observed for low Ni contents whereas on binary $CeNi_xO_y$ solids the first TPR peak has been observed at 264 °C [14]. When x increases up to 2 a second peak at about 385 °C increases. For higher Ni contents, the first peak decreases while the second peak shifts to higher temperatures (418 °C). A linear relationship is obtained between the total hydrogen consumed during TPR with the Ni content of the $CeZr_{0.5}Ni_xO_y$ and $CeNi_xO_y$ compounds (Fig. 7), showing that H_2 is consumed in majority to reduce nickel species. However, it has been shown that NiO facilitates the reduction of a cerium solid solution [2]. Moreover, the difference observed between NiO and $CeNi_xO_y$ reduction temperature was attributed to the presence of small crystallites which are more easily reduced [12]. A series of reactions have been proposed accounting for the reduction mechanism that take place in the solid solution. Redox processes between Ce^{4+}, Ce^{3+}, Ni^0 and Ni^{2+} have been demonstrated [9,12]. These Ni species present the characteristic of being able to be reduced and reoxidized easily and reversibly allowed by their close interaction with Ce species. Therefore it can be proposed that the TPR peaks correspond to the reduction of nickel species in various environments. The low temperature peak could be attributed to nickel species: (i) belonging to the solid solution and/or to (ii) small NiO crystallites, easily reducible, but with the simultaneous reoxidation of a part of these species by reduction of the Ce^{4+} ions in their vicinity into Ce^{3+} species as well as a probable reduction of some Zr^{4+} ions in their vicinity into Zr^{3+}. Then the larger NiO crystallites are reduced when increasing temperature.

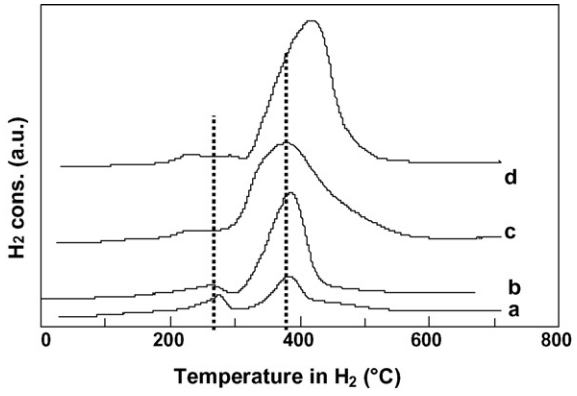

Fig. 6. TPR of (a) $CeZr_{0.5}Ni_{0.3}O_y$, (b) $CeZr_{0.5}Ni_1O_y$, (c) $CeZr_{0.5}Ni_2O_y$ and (d) $CeZr_{0.5}Ni_3O_y$.

3.4. Catalytic partial oxidation of CH_4

Partial oxidation of CH_4 has been studied as a function of the reaction temperature, the activation treatment in H_2 and the metal loading of $CeZr_{0.5}Ni_xO_y$ catalysts. Fig. 8 shows, as an example, the results obtained on the $CeZr_{0.5}Ni_3O_y$ solid versus temperature. For low reaction temperatures where CH_4 and O_2 conversions are obtained without products reported, it has to be recalled that carbon is formed (verified by microanalysis and XPS), and H_2O is produced. H_2 and CO are obtained at high temperatures (≥600 °C), and this is almost the case for CO_2. As shown in Fig. 9, when the solid is previously in situ treated in H_2 at 200 °C during 10 h, H_2 and CO can be obtained at low temperature. Moreover, as CH_4 conversion is almost stable it appears that the active sites created during the activation treatment are stable with temperature. On $CeZr_{0.5}Ni_3O_y$, a methane conversion of 52% is obtained with a H_2 selectivity of about 60% at 200 °C. So, the treatment in H_2 at 200 °C of the solid has a dramatic effect on H_2 production from CH_4 at low temperature [15]. The catalytic results obtained depend on the Ni content of the $CeZr_{0.5}Ni_xO_y$ compounds. In the applied conditions, at 200 °C, a stable H_2 yield of 34% can be observed on $CeZr_{0.5}Ni_2O_y$ with a methane conversion of 53% and a H_2 selectivity of 64%. Therefore, H_2 activity obtained at 200 °C is presented in Fig. 10 as a function of the Ni/M_T molar ratio of the catalysts previously in situ treated in H_2 at 200 °C. Among the solids studied, at 200 °C an

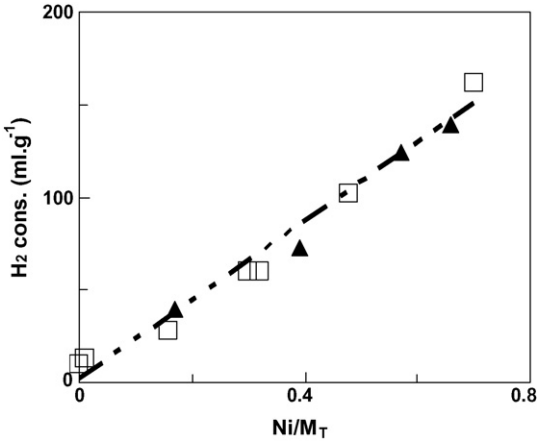

Fig. 7. H_2 consumed during TPR versus Ni content of $CeNi_xO_y$ (□) and $CeZr_{0.5}Ni_xO_y$ (▲) compounds.

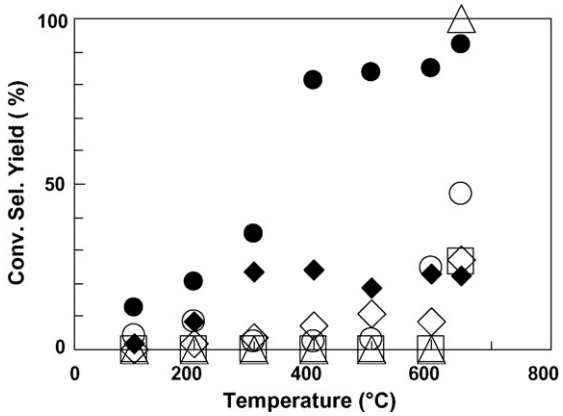

Fig. 8. CH_4 (◆) and O_2 (●) conversions, H_2 (△) CO (○) and CO_2 (◇) selectivities, and H_2 yield (□) as a function of the reaction temperature on $CeZr_{0.5}Ni_3O_y$.

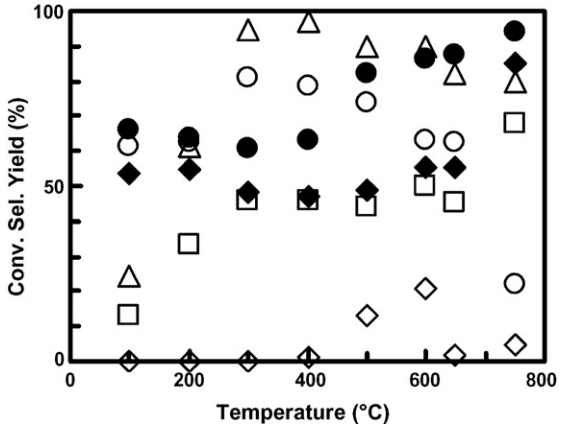

Fig. 9. CH_4 (◆) and O_2 (●) conversions, H_2 (△) CO (○) and CO_2 (◇) selectivities, and H_2 yield (□) as a function of the reaction temperature on $CeZr_{0.5}Ni_3O_y$ in situ previously in situ treated in H_2 at 200 °C.

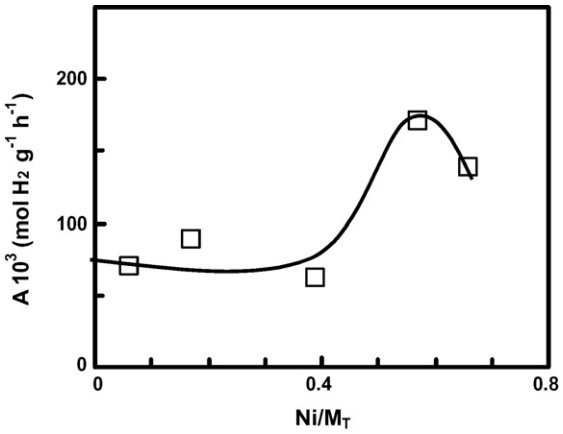

Fig. 10. H_2 activity obtained at 200 °C versus Ni/M_T ratio of the $CeZr_{0.5}Ni_xO_y$ solids previously in situ treated in H_2 at 200 °C.

optimum H_2 yield is obtained for a Ni/M_T ratio of about 0.55 corresponding to the $CeZr_{0.5}Ni_2O_y$ catalyst, while at 700 °C a H_2 yield of 100% is obtained on this compound with or without previous treatment in H_2, showing very good catalytic results at high temperature as already reported in the literature [1,2]. Moreover, as the $CeZr_{0.5}Ni_xO_y$ surface areas are relatively similar for the studied series, the catalytic results obtained cannot be related to a variation of this parameter.

H_2 formation activity can be reported in mol $mol(Ni)^{-1}$ s^{-1} as a function of the Ni proportion (Ni/M_T) present in the $CeZr_{0.5}Ni_xO_y$ solids as presented in Fig. 11. H_2 activity reported in mol $mol(Ni)^{-1}$ s^{-1} corresponds to H_2 activity in $molH_2$ g^{-1} s^{-1} divided by the Ni content of the solid. A continuous decrease of the activity is obtained as a function of the Ni content of the solid, whatever the temperature. So the highest proportion of active Ni species is obtained for low Ni contents, i.e., when Ni species are in ceria–zirconia solid solution or forming small NiO particles. Moreover, in the laboratory, a model has been developed on hydrotreating MoS_2 catalysts, allowing correlating the activity to the position of the active sites for different geometrical structures [16]. And, in agreement with this previous study, the curve obtained can be easily explained if the Ni atoms located at the periphery of the NiO crystallites are responsible of the H_2 activity. The proportion of active sites is higher when the NiO crystallites are smaller in agreement with the well-known dispersion

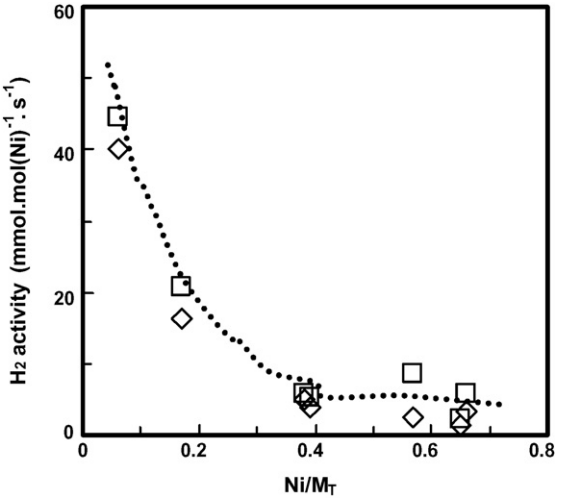

Fig. 11. H_2 activity measured at 100 °C (◇) and 200 °C (□) reported in mol $mol(Ni)^{-1}$ s^{-1} versus Ni/M_T ratio of $CeZr_{0.5}Ni_xO_y$ solids previously in situ treated in H_2 at 200 °C.

influence. Therefore, H_2 activity from POM certainly involves particular sites where Ce, Zr and Ni are in close interaction.

Moreover, the treatment in H_2 at 200 °C leads to a drastic effect on the H_2 yield at low temperature. Interaction of hydrogen with cerium- and nickel-based mixed oxides has already been studied [7,12]. After an in situ treatment in H_2 in particular at 200 °C, it has been reported that the $CeZr_{0.5}Ni_xO_y$ solids studied become large hydrogen reservoirs, called oxyhydrides [7]. Moreover, the hydrogen reservoir is relatively stable with temperature on these particular solids, which can be correlated with the stability of the conversion of CH_4 with temperature, once the active sites are created. The insertion in the solid of particular hydrogen species created by heterolytic splitting of H_2 on an O^{2-} species and an anionic vacancy of the solid has been summarized as follows:

$$O^{2-}M^{n+}\square + H_2 \rightarrow OH^-M^{n+}H^- \quad (1)$$

with □: anionic vacancy, and M^{n+}: cation.

It appears that different kinds of active sites which differ from each other in terms of the environment of Ni can exist. Such a site has already been modeled, by an ensemble of two cations in close interaction whatever in the solid solution or at the NiO and ceria, ceria–zirconia, and/or solid–solution (with Ni) interface (Scheme 1, the number of anionic vacancies presented is arbitrary) [12]. Taking into account that dehydrogenation step requires the abstraction of hydrogen species from the hydrocarbon, the ability of the solid to accept hydrogen can be a prerequisite condition, as it has already been proposed for propane activation on $CeNi_xO_y$ compounds [8]. Therefore, by analogy to the heterolytic dissociation of H_2, the heterolytic dissociation of methane can be envisaged on a low coordination site involving an anionic vacancy (the following equation):

$$2O^{2-}M^{n+}\square + CH_4 \rightarrow 2OH^-M^{n+}H^- + C \quad (2)$$

$$2H^- + O_2 \rightarrow O^{2-} + \square + H_2O \quad (3)$$

$$2OH^- \rightarrow O^{2-} + \square + H_2O \quad (4)$$

The high reactivity of the hydride species permits consumption of O_2 (exothermic) forming water (Eq. (3)), and therefore the solid can present an enhancement at the surface of the hydroxyl groups' concentration; it also permits transformation of O_2 into selective

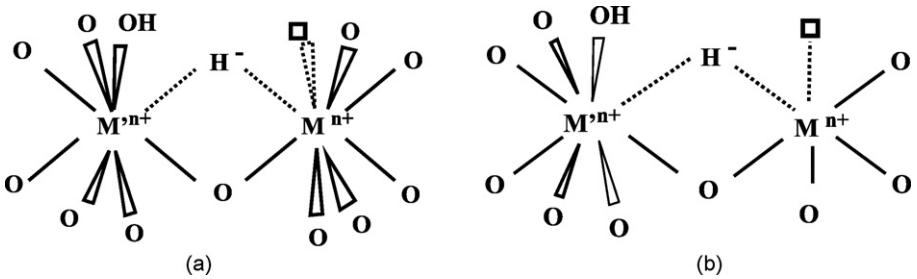

Scheme 1. Active site generated in H_2 on cerium zirconium- and nickel-based mixed oxides (a) in the solid solution (cerium zirconium nickel) and (b) at the NiO crystallite and ceria–zirconia or solid–solution interface. M^{n+} = Ni^{2+}, $Ni^{\delta+}$ and M^{n+} = Ce^{4+}, Ce^{3+}, Zr^{4+}, Zr^{3+}, Ni^{2+}, or $Ni^{\delta+}$. (□) Anionic vacancy (number arbitrary).

oxygen species O^{2-}, which regenerates the active site (Eq. (4)). This phenomenon can explain the low level of total oxidation (CO_2) but CO is formed so carbon oxidation has also to be considered.

4. Conclusion

The partial oxidation of CH_4 has been studied on $CeZr_{0.5}Ni_xO_y$ ($0 < x \leq 3$) catalysts. Hydrogen can be produced at low temperature (200 °C) over $CeZr_{0.5}Ni_xO_y$ oxyhydrides i.e. mixed oxides previously in situ treated in H_2 at 200 °C. Ion sputtering followed by XPS analysis evidences small NiO crystallites (10–15 Å) present in the compounds. The active nickel species belongs to these small crystallites and/or to the cerium zirconium nickel solid solution where Ni species are in close interaction with Ce or Zr species permitting a redox process. These Ni species present the characteristic of being able to be reduced and reoxidized easily and reversibly. While the dehydrogenation step requires the abstraction of hydrogen from the hydrocarbon, by analogy to the heterolytic dissociation of H_2, an active site is proposed based on the presence of anionic vacancies able to abstract hydride species from methane.

References

[1] T. Zhu, M. Flytzani-Stephanopoulos, Appl. Catal. 208 (2001) 403.
[2] S. Xu, X. Wang, Fuel 84 (2005) 563.
[3] V.R. Choudhary, V.H. Rane, A.M. Rajput, Catal. Lett. 22 (1993) 289.
[4] W. Shan, M. Luo, P. Ying, W. Shen, C. Li, Appl. Catal. 246 (2003) 1.
[5] H.S. Roh, K.W. Jun, S.S.H. Beak, S.E. Park, Chem. Lett. 10 (2001) 1048.
[6] V.R. Choudhary, V.H. Rane, A.M. Rajput, US005411927A Patent, 1995.
[7] L. Jalowiecki-Duhamel, J. Carpentier, A. Ponchel, Int. J. Hydrogen Energy 32 (2007) 2439.
[8] L. Jalowiecki-Duhamel, A. Ponchel, C. Lamonier, A. D'Huysser, Y. Barbaux, Langmuir 17 (2001) 1511.
[9] A. Ponchel, A. D'Huysser, C. Lamonier, L. Jalowiecki-Duhamel, Phys. Chem. Chem. Phys. 2 (2000) 303.
[10] G. Wrobel, M.P. Sohier, A. D'Huysser, J.P. Bonnelle, J.P. Marcq, Appl. Catal. 101 (1993) 73.
[11] G. Wrobel, C. Lamonier, A. Bennani, A. D'Huysser, A. Aboukaïs, J. Chem. Soc., Faraday Trans. 92 (1996) 2001.
[12] C. Lamonier, A. Ponchel, A. D'Huysser, L. Jalowiecki-Duhamel, Catal. Today 50 (1999) 247.
[13] T.L. Barr, in: N.S. McIntyre (Ed.), Quantitative Surface Analysis of Materials, ASTM 643, American Society for Testing and Materials, 1978, p. 83.
[14] L. Jalowiecki-Duhamel, H. Zarrou, A. D'Huysser, in: Proceedings of the IHEC 2007, Istanbul, Turkey, 2007.
[15] H. Zarrou, L. Duhamel, W02006045951, Patent to CNRS and University Lille 1, 2006.
[16] S. Kasztelan, H. Toulhoat, J. Grimblot, J.P. Bonnelle, Appl. Catal. 13 (1984) 127.